J Therm Anal Calorim (2014) 118:1585–1592
DOI 10.1007/s10973-014-4073-z

Thermal study in Eu^{3+}-doped boehmite nanofibers and luminescence properties of the corresponding Eu^{3+}:Al_2O_3

Xiangyu Xu · Yuxin Liu · Zhi Lv · Jiaqing Song · Mingyuan He · Qian Wang · Lijun Yan · Zhaofei Li

Received: 12 May 2014 / Accepted: 3 August 2014 / Published online: 29 August 2014

Abstract Eu^{3+}-doped boehmite nanofiber materials with different Eu^{3+} concentrations were synthesized without any surfactant, and followed by a series of characterizations. It was found that the boehmite nanofibers became coarser with the increase of Eu^{3+} concentration, which resulted in a gradual decrease of their specific surface areas. Moreover, the thermal stability of the boehmite nanofibers was studied by thermogravimetry–differential scanning calorimetry. All materials showed the phase transition from γ-Al_2O_3 to other forms. Yet the transition temperature was increased with the increase of Eu^{3+} concentration. The Eu^{3+}-doped boehmite nanofibers with the maximum Eu^{3+} concentrations showed the best thermal stability. Photoluminescence spectra showed that the 2 mol% of doping concentration of Eu^{3+} ions in Eu^{3+}:-Al_2O_3 nanofiber was optimum.

Keywords Boehmite · Nanofibers · Al_2O_3 · Europium

X. Xu · Y. Liu · Z. Lv · J. Song (✉)
State Key Laboratory of Chemical Resource Engineering, Beijing University of Chemical Technology, Beijing 100029, China
e-mail: songjq@126.com

M. He
Shanghai Key Laboratory of Green Chemistry and Chemical Processes, East China Normal University, Shanghai 200062, China

Q. Wang · L. Yan · Z. Li
Petrochemical Research Institute of Petrochina, Beijing 100195, China

Introduction

Rare earth (RE) ion doped in different host materials have drawn great attention for the applications of these materials in phosphors, optical amplifiers, medical labeling, imaging, radiation detection, etc. [1–3]. The macroscopic properties of phosphors, such as the emission spectrum or the luminous efficiency, rely on their composition, crystal structure, and microstructure [4–9]. It was reported that the shape of nanoscale materials had a pronounced influence on their physicochemical properties [10–12]. Hence, it is necessary and important to control morphology of the materials.

Among the host materials, alumina (Al_2O_3) has been investigated as a suitable host for RE ions, due to its high optical transparency in the spectral range from ultraviolet to near-infrared (IR), excellent mechanical properties, and good chemical stability [13–15]. Boehmite (AlO(OH)) as a raw material is widely applied for producing γ-Al_2O_3 and α-Al_2O_3 [16–18]. To date, well-defined AlOOH nanostructures with various morphologies such as nanofibers [19, 20], nanorods and nanoflakes [21], nanotubes [22], nanobelts [23] and their assemblies have been prepared by a variety of methods, including direct solution precipitation [24], sol–gel synthesis [25], spray pyrolysis, and hydrothermal treatment [26, 27]. In particular, the synthesis methodology of the nanofibrous boehmite is especially important for preparing nanofibrous alumina because of its large specific surface area and large pore volume [28, 29]. The specific surface area and the pore volume of Al_2O_3 obtained after 1,200 °C calcination can attain certain values due to the high retention of its fibrous shape. There are several studies reported in Eu:Al_2O_3 materials. However, the variations in the morphology and the thermal stability of Eu^{3+}-doped alumina nanofibers have not been reported.

Peng et al. [30] and Li and colleagues [31] reported that boehmite nanofibers were successfully prepared via a soft chemical hydrothermal treatment without using any surfactant, solvent, or hard templates. Based on Peng's and Li's work, Xu et al. [32] reported the variations in the morphology and the thermal stability of fibrous crystallites of boehmites prepared at different hydrothermal temperatures. Europium is one of lanthanides which are widely used for fabrication of red-emitting materials [33]. In this paper, Eu^{3+}-doped alumina nanofibers were synthesized with different europium concentrations, and their thermal stabilities and luminescence properties were studied.

Experimental

Preparation of the Eu^{3+}-doped alumina nanofibers

Different concentrations of europium-doped boehmites nanofibers were synthesized by hydrothermal conditions. Different amounts of $Eu(NO_3)_3{\cdot}6H_2O$ (the molar ratio of Eu^{3+} to Al_2O_3 is 0, 1, 2, and 3 mol%) were added into 0.5 mol kg^{-1} $Al_2(SO_4)_3{\cdot}18H_2O$ solution and mixed homogeneous to form solution A. $NaAlO_2$ solution, which was prepared by aluminum hydroxide and sodium hydroxide with the molar ratio of 5.2 for Na^+:Al^{3+}, was added dropwise to solution A with stirring, and the stirring was maintained until the pH reached 9.0. The suspension was transferred into a Teflon-lined stainless autoclave, then kept in oven stationary at 150 °C for 24 h. The resulting precipitate was recovered by centrifugation, washed with pure water several times to remove sodium sulfate and then dried in air at 80 °C to obtain the Eu^{3+}-doped boehmite nanofibers. In order to obtain the Eu^{3+}-doped alumina nanofibers, calcination was conducted in muffle furnace.

Analysis and characterization

X-ray powder diffraction (XRD) patterns were recorded on a Rigaku D/MAX 2500 X-ray diffractometer with a graphite monochromator and Cu Kα radiation ($\lambda = 1.54178$ Å). The Fourier transform IR spectroscopy (FT-IR) was performed at room temperature by means of VECTOR 22 spectrometer in the frequency range of 400–4,000 cm^{-1}. Scanning electron microscopy (SEM) images were obtained using a ZEISS SUPER 55 scanning electron microscope. Transmission electron microscopy (TEM) images were obtained on a JEM-2100 electron microscopy. A small amount of samples was first dispersed ultrasonically in alcohol and then dropped onto the lacey support films prior to the observation. The specific surface area was measured using the N_2 sorption method with a Micromeritics ASAP 202 instrument. Thermal gravimetric analysis and differential scanning calorimetry (TG–DSC) of the products were recorded using a METTLER TOLEDO TGA/DSC1/1100SF. Samples were heated in a flowing air from room temperature to 1,000 °C with a heating rate at 10 °C min^{-1}. Photoluminescence (PL) spectra are measured with a Hitachi F7000 fluorescence spectrophotometer. The light from a 450 W xenon lamp through the monochromator is used for the optical excitation.

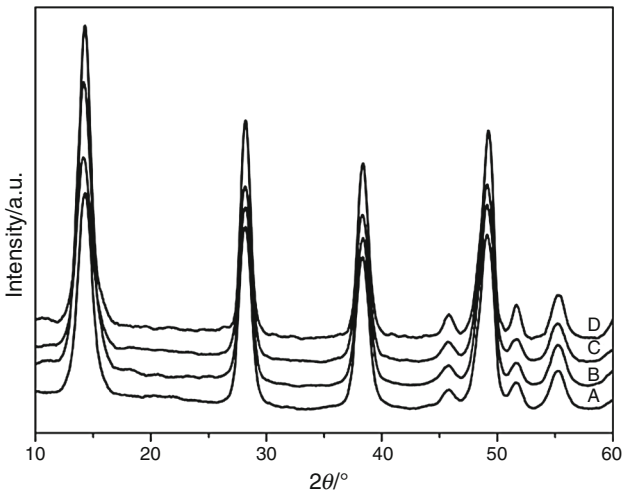

Fig. 1 XRD patterns of the Eu^{3+}-doped boehmite nanofibers with different europium concentrations. (*A*) 0 mol%, (*B*) 1 mol%, (*C*) 2 mol%, and (*D*) 3 mol%

Results and discussions

The powder XRD patterns of the Eu^{3+}-doped boehmite nanofibers with different europium concentrations are shown in Fig. 1. It could be seen that all patterns exhibited typical reflections of boehmite phase (Ref: JCPDS no. 74-1895) without any impurity peak. The strong sharp reflections indicate that the Eu^{3+}-doped boehmite nanofibers have a well-formed crystalline structure. It was implied that the Eu^{3+}-doped boehmite nanofibers with different europium concentrations had been prepared successfully. Obvious differences among the samples with different europium concentrations were not observed. The powder XRD patterns of the Eu^{3+}-doped boehmite nanofibers (2 mol%) and samples obtained at 400, 600, 800, 1,000, and 1,200 °C are shown in Fig. 2. It could be seen that the patterns of the sample obtained at 400 °C were the same as that of the Eu^{3+}-doped boehmite, which indicating that the Eu^{3+}-doped boehmite nanofibers were stable at 400 °C. When the calcination temperature was raised to 600 °C, the boehmite structure changed to γ-Al_2O_3 (Ref: JCPDS no. 10-0425), which could be well maintained with the calcination temperature up to 800 °C,

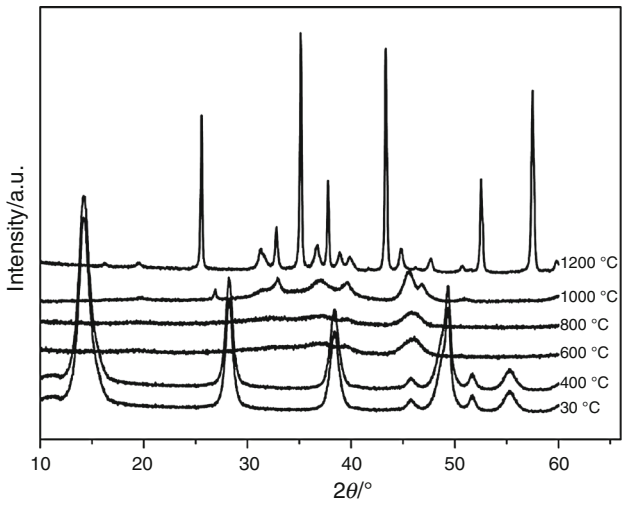

Fig. 2 XRD patterns of the Eu^{3+}-doped boehmite nanofibers (2 mol%) and samples obtained at different calcination temperatures

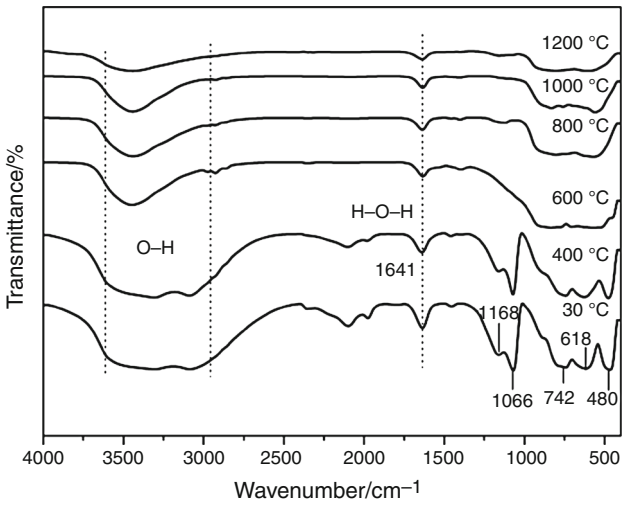

Fig. 4 FT-IR spectra of the Eu^{3+}-doped boehmite nanofibers (2 mol%) and samples obtained at different calcination temperatures

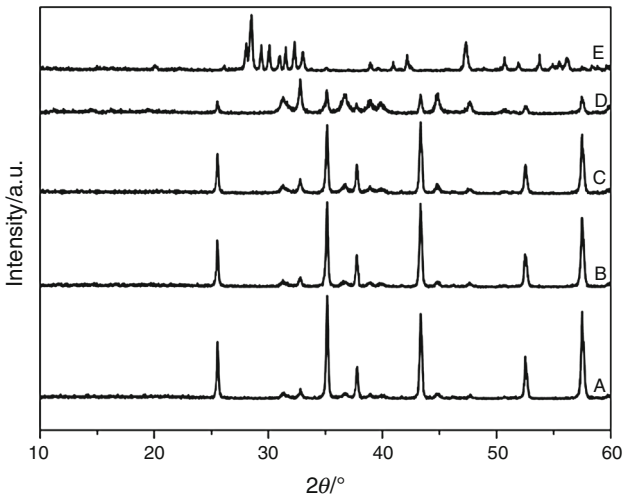

Fig. 3 XRD patterns of Al_2O_3:Eu^{3+} calcined at 1,200 °C for 3 h with different europium concentrations. (*A*) 0 mol%, (*B*) 1 mol%, (*C*) 2 mol%, (*D*) 3 mol%, and (*E*) Eu_2O_3

as shown in Fig. 2; δ-Al_2O_3 emerged when the calcinations temperature reached 1,000 °C. With a further increase of the calcination temperature from 1,000 to 1,200 °C, the mixture of θ-Al_2O_3 (Ref: JCPDS no. 35-0121) and α-Al_2O_3 (Ref: JCPDS no. 10-173) was confirmed.

Figure 3 presents the XRD patterns of Al_2O_3 and europium-doped Al_2O_3 containing different amounts of europium calcined at 1,200 °C for 3 h. It could be seen that all four samples with different amounts of europium exhibited similar reflections of mixed phases with θ-Al_2O_3 (Ref: JCPDS no. 35-0121) and α-Al_2O_3 (Ref: JCPDS no. 10-173). No Eu_2O_3 phase was found, because the concentration of Eu^{3+} was low, and furthermore, Eu^{3+} ions could incorporate into Al_2O_3 lattice and formed substituted solid solution [4].

The FT-IR spectra of the Eu^{3+}-doped boehmite nanofibers (2 mol%) and samples obtained at different calcination temperatures are shown in Fig. 4. The wide band at 3,000–3,500 cm^{-1} and the sharp band at 1,642 cm^{-1} in the FT-IR spectrum for the Eu^{3+}-doped boehmite nanofibers sample (Fig. 4, curve 30 °C) were due to the existence of adsorbed water and structural water in boehmite [34]. The band at 1,066 cm^{-1} and the shoulder at 1,168 cm^{-1} could be assigned to the δ_s Al–O–H and δ_{as} Al–O–H mode of boehmite [35]. The three bands at 742, 618 and 480 cm^{-1} represented the vibration mode of AlO_6 [36]. In the case of sample obtained at 400 °C (Fig. 4, curve 400 °C), it could be seen that there was almost same as that of the Eu^{3+}-doped boehmite nanofibers. This indicated that the Eu^{3+}-doped boehmite nanofibers were stable at 400 °C, which was in agreement with the XRD results, as shown in Fig. 2. When the calcination temperature was raised to 600 °C, the band at 3,000–3,500 cm^{-1} of adsorbed water and structural water became narrower and the peak at 1,642 cm^{-1} got weaker, which suggested the loss of water.

Figure 5 shows the TEM images of the Eu^{3+}-doped boehmite nanofibers (2 mol%) and the samples calcined at 400, 600, 800, 1,000, and 1,200 °C, respectively. The corresponding particle sizes are shown in Table 1. It could be seen that the starting Eu^{3+}-doped boehmite nanofibers had a length over 150 nm and an average diameter of about 14 nm (Fig. 5a). All the samples obtained at different temperatures showed similar fibrous morphology, even at 1,200 °C. It implied that the fibrous structure had a certain resistance to sintering even if they were calcined at high

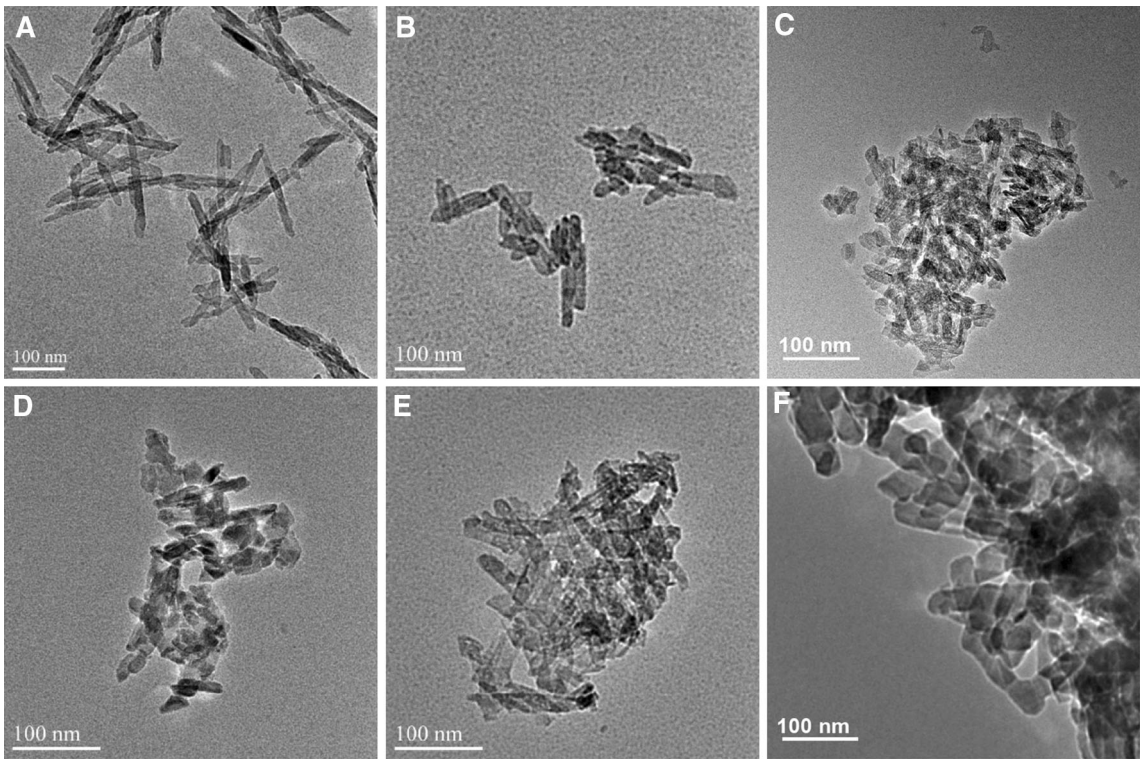

Fig. 5 TEM images of **a** the AlOOH:Eu^{3+} (2 mol%) boehmite nanofibers and calcined at **b** 400 °C, **c** 600 °C, **d** 800 °C, **e** 1,000 °C, and **f** 1,200 °C

Table 1 Properties of the Eu^{3+}-doped boehmite nanofibers (2 mol%) and samples obtained at different calcination temperatures

T/°C	$S_{BET}/m^2\ g^{-1}$	*D*/nm (Average figures)
30	161.6	13.6
400	170.7	16.7
600	198.5	14.3
800	149.3	20.2
1,000	86.4	21.5
1,200	43.7	30.6

temperatures. When the sample was calcined at 400 °C for 2 h, the nanofibers were about 17 nm in diameter and 100 nm in length. The diameter of nanofibers was about 14 nm after calcined at 600 °C. This was related to the combined effect of dehydration and condensation. The phase transition was accompanied by a decrease in the size of the crystallites [30]. With the increase of the calcination temperature, the average diameter of the Al_2O_3 nanofibers was enlarged from 14 nm at 600 °C to 30 nm at 1,200 °C while the length was reduced simultaneously.

The specific surface areas of the Eu^{3+}-doped boehmite nanofibers (2 mol%) and samples obtained at different calcination temperatures are shown in Table 1. It could be seen that there was an increase of specific surface area with the increase of calcination temperature from 30 to 600 °C. This was related to the phase conversion, which was followed by a decrease in the size of the crystallites and a corresponding increase in the specific surface area. It could be seen that there was a descending trend for the specific surface area as the calcination temperature increased from 600 to 1,200 °C. The first event in the temperature range 600–800 °C was attributed to the coarsening and shortening of γ-Al_2O_3 nanofibers. The second event from 800 to 1,200 °C is due to the transition of γ–α-Al_2O_3 and the coarsening of Al_2O_3 nanofibers. The transition of γ–α-Al_2O_3 involves a reconstructive recrystallization process, which leads to the minor sinter of the fibrous structure.

The TEM images of the Eu^{3+}-doped boehmite nanofibers with different doping concentrations are shown in Fig. 6. Table 2 shows the corresponding particle sizes and the BET surface areas. As could be seen in Table 2, there was an ascending trend for the particle sizes and a descending trend for the specific surface area with the increase of Eu^{3+}-doped concentrations from 0 to 3 %. The decrease of the specific surface area was related to the increase of particle sizes of the nanofibers.

The mass losses of the Eu^{3+}-doped boehmite nanofibers with different europium concentrations were measured by TG–DSC method to investigate their thermal behavior. The measured TG–DSC–DTG curves of the four nanofibers are

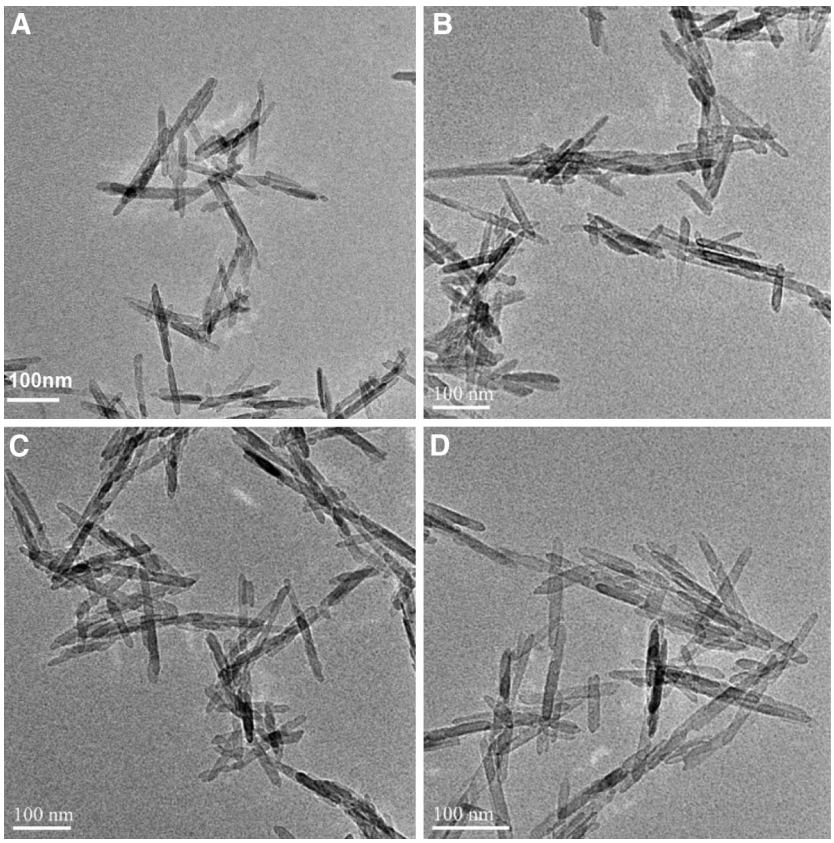

Fig. 6 TEM images of the AlOOH:Eu^{3+} boehmite nanofibers with different europium concentrations. **a** 0 mol%, **b** 1 mol%, **c** 2 mol%, and **d** 3 mol%

Table 2 Properties of the AlOOH: Eu^{3+} boehmite nanofibers with different europium concentrations

Eu^{3+} concentrations/mol %$^{-1}$	S_{BET}/m^2 g^{-1}	D/nm (Average figures)
0	241.5	11.6
1	210.4	12.4
2	161.6	13.6
3	147.2	15.4

shown in Fig. 7. As shown in Fig. 7, curve a exhibited three mass losses steps according to the TG curve with the total mass losses of 27.5 % and corresponding endothermic peaks in the DSC curve. The endothermic peak centered at 110 °C with the associated mass loss of 3.65 % was corresponded to the removal of surface adsorbed water. A second mass loss at 230–639 °C with an endothermic peak centered at 468 °C could be attributed to the removal of the hydroxyl group, which corresponded to the lattice changes coinciding with the transformation of boehmite to γ-Al_2O_3 [37, 38]. This was in agreement with the XRD results, as shown in Fig. 2. The last event was ascribed to the further dehydroxylation of the γ-Al_2O_3 and the formation of δ-Al_2O_3 [39–42].

It could be seen from Fig. 7, curves b–d, that all three Eu^{3+}-doped boehmite nanofibers exhibited similar TG–DSC curve as that of boehmite nanofibers. However, in the DSC curves of the three Eu^{3+}-doped boehmite nanofibers, the first endothermic peaks were not clearly observed as that of curve a, which were ascribed to the losses of surface adsorbed water. The associated mass losses were 3.65, 3.11, 2.92, and 2.85 %, respectively, with the increase of europium concentrations from 0 to 3. As shown in Fig. 7, with the increase of europium concentrations from 0 to 3, the endothermic peaks which corresponded to the transformation of boehmite to γ-Al_2O_3 in DSC curve centered at about 468, 505, 507, and 509 °C, respectively, and the total mass losses were 27.5, 20, 18.1, and 17.4 %, respectively. The variation of phase transition temperature was due to high surface energy, which caused by large surface area results in instability of the boehmite nanofibers. The different total loss was proposed as follows: the Eu^{3+} entered into the interstitial positions of the lattice of boehmite nanofibers and decreased the oxygen vacancies, which would decrease the amount of hydroxyl group and surface adsorbed water.

In short, the increase of europium concentrations brought about the increase of particle size, which caused

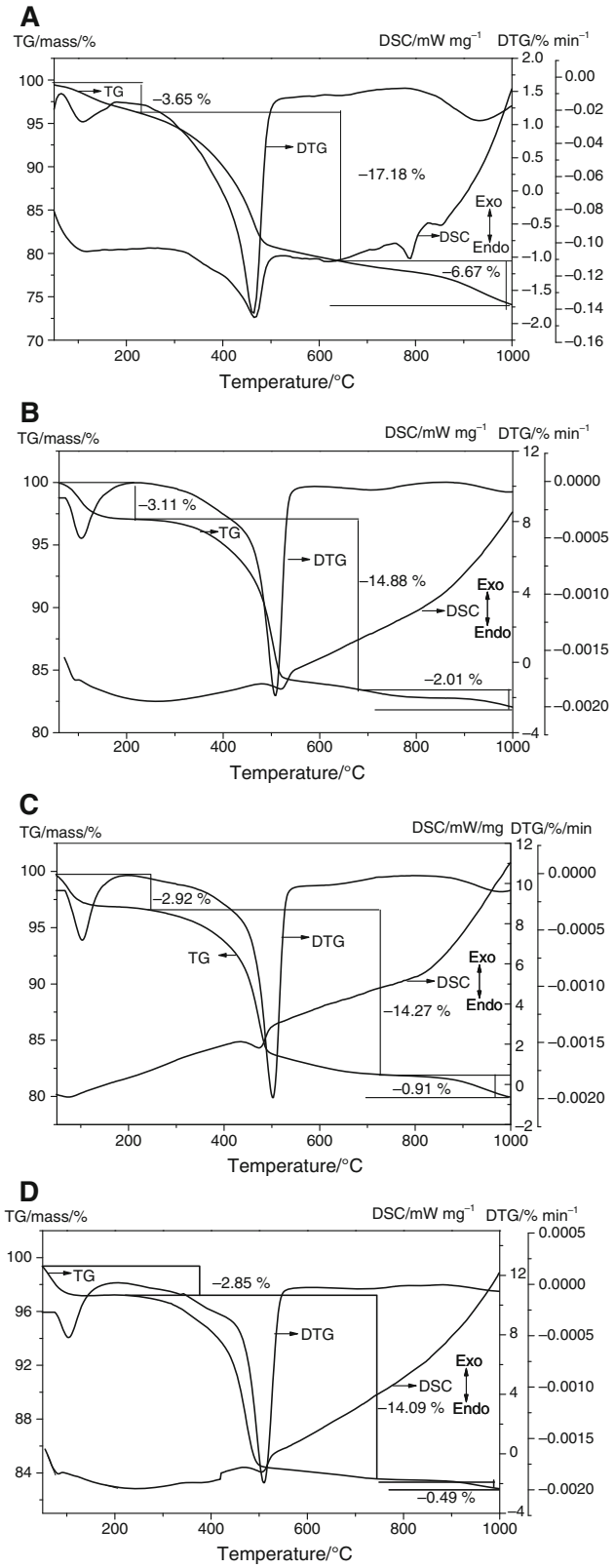

Fig. 7 TG–DTG–DSC of the Eu^{3+}-doped boehmite nanofibers with different europium concentrations. **a** 0 mol%, **b** 1 mol%, **c** 2 mol%, and **d** 3 mol%

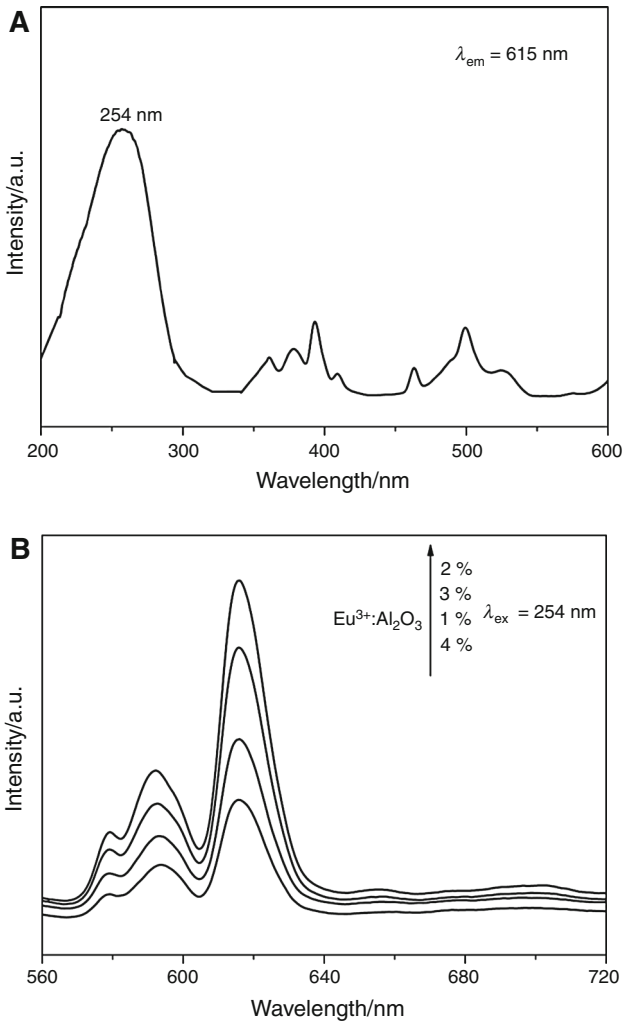

Fig. 8 **a** Excitation spectrum of the Eu^{3+}-doped alumina nanofibers prepared at 800 °C for 3 h (Eu^{3+}:Al_2O_3 = 2 mol%, λ_{em} = 615 nm), **b** emission spectra of the various Eu^{3+}:Al_2O_3 ratio prepared at 800 °C for 3 h (Eu^{3+}:Al_2O_3 = *x* mol%, λ_{ex} = 254 nm)

the decrease of the surface area and brought about the increase in the transition temperatures. This indicated that the europium concentrations of the nanofibers played an important role on thermal stability.

Due to the similarities in PLE spectra of the samples with different Eu^{3+} concentrations, typical spectrum of Al_2O_3 nanofibers with 2 mol% Eu^{3+} content is shown in Fig. 8a. The PLE spectrum monitored at 615 nm presented a series of intra-configurational transitions of Eu^{3+}. It could be seen that the peak centered at 254 nm was the most intensive, so 254 nm was chosen as the excitation wavelength. Figure 8b shows the PL spectra of Al_2O_3:Eu^{3+} nanofibers synthesized at 800 °C for 3 h with different Eu^{3+}:Al_2O_3 ratio (Eu^{3+}:Al_2O_3 = 1, 2, 3, 4 mol%). As shown in Fig. 8b, upon excitation at 254 nm, the characteristic emission spectrum of $^5D_0 \rightarrow {}^7F_J$ transitions for the Eu^{3+} ion [43] could be clearly observed. They could be

related to the transitions from the $^5D_0$ state to ^7F_J ($J = 0$, 1, 2, 3, 4) states at 579, 592, 615, 633, and 700 nm. Furthermore, for all samples, the $^5D_0 \rightarrow {}^7F_2$ (615 nm) band was the most intensive. It could be seen that the emission intensity strongly depended on the doping concentration. The best optimum concentration was found to be 2 mol%. Below this concentration, the emission intensity was weak because no sufficient luminescent centers were applied. For higher doping, the intensity was also reduced due to the quenching. The emission band at 592 nm, which corresponds to the $^5D_0 \rightarrow {}^7F_1$, was a magnetic dipole one and hardly varies with the crystal filed strength around Eu^{3+} ion. However, the transition $^5D_0 \rightarrow {}^7F_2$ at 615 nm was electric dipole transition limited by the symmetry constraint. The ($^5D_0 \rightarrow {}^7F_2$)/($^5D_0 \rightarrow {}^7F_1$) intensity ratio suggested that europium ion occupied low symmetry sites.

Conclusions

In this study, the variations in the thermal stability of Eu^{3+}-doped boehmite nanofibers prepared with different Eu^{3+} concentrations and the luminescence of the corresponding Eu^{3+}:Al_2O_3 were investigated. With the increase of the Eu^{3+} concentrations from 0 to 3, the average diameter of the boehmite nanofibers increased from 11.6 to 15.4 nm, inducing a gradual decrease of the specific surface area from 241.5 to 147.2 $m^2\ g^{-1}$. This brought about the increase of the phase transition temperature. PL spectra showed that upon excitation at 254 nm, the asymmetry ratio of ($^5D_0 \rightarrow {}^7F_2$)/($^5D_0 \rightarrow {}^7F_1$) intensity suggested that europium ion occupied low symmetry sites. It was shown that the 2 mol% of doping concentration of Eu^{3+} ions in Eu^{3+}:Al_2O_3 nanofiber was optimum.

Acknowledgements We are grateful to the financial support from 863 Program (2009AA064201) and National Science and Technology Support Program (2012BAE05B02).

References

1. Monteiro MAF, Brito HF, Felinto M. Photoluminescence behavior of Eu^{3+} ion doped into γ-and α-alumina systems prepared by combustion, ceramic and Pechini methods. Microporous Mesoporous Mater. 2008;108:237–46.
2. Ningthoujam RS, Sudarsan V, Godbole SV. SnO_2:Eu^{3+} nanoparticles dispersed in TiO_2 matrix: improved energy transfer between semiconductor host and Eu^{3+} ions for the low temperature synthesized samples. Appl Phys Lett. 2007;90:173113.
3. Chang YT, Chang HL, Su KW. High-efficiency Q-switched dual-wavelength emission at 1176 and 559 nm with intracavity Raman and sum-frequency generation. Opt Express. 2009;17:11892–7.
4. Liu D, Zhu Z. Photoluminescence properties of the Eu-doped alpha-Al_2O_3 microspheres. J Alloys Compd. 2014;583:291–4.
5. Wang D, Yang P, Cheng Z. Patterning of $Gd_2(WO_4)_3$:Ln^{3+} (Ln = Eu, Tb) luminescent films by microcontact printing route. J Colloid Interface Sci. 2012;365:320–5.
6. Zhou JC, Sun LD, Shen J. Fluorescent-magnetic nanocrystals: synthesis and property of $YP_xV_{1-x}O_4$:Eu@$GdPO_4$ core/shell structure. Nanoscale. 2011;3:1977–83.
7. Yu T, Joo J, Park YI. Large-scale nonhydrolytic sol–gel synthesis of uniform-sized ceria nanocrystals with spherical, wire, and tadpole shapes. Angew Chem Int Ed. 2005;117:7577–80.
8. Zhu Z, Liu D, Liu H. Photoluminescence properties of Tb^{3+} doped Al_2O_3 microfibers via a hydrothermal route followed by heat treatment. Ceram Int. 2012;38:4137–41.
9. Jiang XC, Sun LD, Yan CH. Ordered nanosheet-based YBO_3:-Eu^{3+} assemblies: synthesis and tunable luminescent properties. J Phys Chem B. 2004;108:3387–90.
10. Boyer D, Mahiou R. Powders and coatings of $LiYF_4$:Eu^{3+} obtained via an original way based on the sol–gel process. Chem Mater. 2004;16:2518–21.
11. Yu L, Li D, Yue M. Dependence of morphology and photoluminescent properties of $GdPO_4$:Eu^{3+} nanostructures on synthesis condition. Chem Phys. 2006;326:478–82.
12. Jia CJ, Sun LD, You LP. Selective synthesis of monazite-and zircon-type $LaVO_4$ nanocrystals. J Phys Chem B. 2005;109:3284–90.
13. Church JS, Cant NW, Trimm DL. Stabilization of aluminas by rare earth and alkaline earth ions. Appl Catal A. 1993;101:105–16.
14. Kumar K-NP, Tranto J, Kumar J, Engell JE. Pore-structure stability and phase transformation in pure and M-doped (M = La, Ce, Nd, Gd, Cu, Fe) alumina membranes and catalyst supports. J Mater Sci Lett. 1996;15:266–70.
15. Ozawa M, Nishio Y. Thermal stabilization of γ-alumina with modification of lanthanum through homogeneous precipitation. J Alloys Compd. 2004;374:397–400.
16. Yu PC, Yang RJ, Chang YT, Yen FS. Fabrication of nano-scaled α-Al_2O_3 crystallites through heterogeneous precipitation of boehmite in a well-dispersed θ-Al_2O_3 suspension. J Am Ceram Soc. 2007;90:2304–46.
17. Chin SY, Lin FJ, Ko AN. Vapour phase hydrogenation of cinnamaldehyde over Ni/γ-Al_2O_3 catalysts: interesting reaction network. Catal Lett. 2009;132:389–94.
18. Martinez A, Prieto G, Rollan J. Nanofibrous γ-Al_2O_3 as support for Co-based Fischer–Tropsch catalysts: pondering the relevance of diffusional and dispersion effects on catalytic performance. J Catal. 2009;263:292–305.
19. Li YY, Liu JP, Jia ZJ. Fabrication of boehmite AlOOH nanofibers by a simple hydrothermal process. Mater Lett. 2006;60:3586–90.
20. Zhao Y, Frost RL, Martens WN, Zhu HY. XRD, TEM and thermal analysis of Fe doped boehmite nanofibres and nanosheets. J Therm Anal Calorim. 2007;90:755–60.
21. Chen XY, Lee SW. pH-Dependent formation of boehmite (γ-AlOOH) nanorods and nanoflakes. Chem Phys Lett. 2007;438:279–84.
22. Hou HW, Xie Y, Yang Q, Guo QX, Tan CR. Preparation and characterization of γ-AlOOH nanotubes and nanorods. Nanotechnology. 2005;16:741–5.
23. Gao P, Xie Y, Chen Y, Ye LN, Guo QX. Large-area synthesis of single-crystal boehmite nanobelts with high luminescent properties. J Cryst Growth. 2005;285:555–60.
24. Kuiry SC, Megen Ed, Patil SD, Deshpande SA, Seal S. Solution-based chemical synthesis of boehmite nanofibers and alumina nanorods. J Phys Chem B. 2005;109:3868–72.
25. Kakade MB, Ramanathan S, Kothiyal GP. Nano-alumina by gel combustion, its thermal characterization and slurry-based coating on stainless steel surface. J Therm Anal Calorim. 2013;112:133–40.

26. Taobo H, Lan X, Shen LZ. Different nanostructures of boehmite fabricated by hydrothermal process: effects of pH and anions. CrystEngComm. 2009;11:1338–42.
27. Palou MT, Bagel L, Zivica V, Marta K, Tomas I. Hydration of high alumina cement–silica fume composite with addition of Portland cement or sodium polyphosphate under hydrothermal treatment. J Therm Anal Calorim. 2013;113:385–94.
28. Zhao YY, Frost RL, Martens WN, Zhu HY. Growth and surface properties of boehmite nanofibers and nanotubes at low temperatures using a hydrothermal synthesis route. Langmuir. 2007;23:9850–9.
29. Hu XF, Liu YQ, Tang Z, Li GC, Zhao RY. Fabrication of high surface area γ-alumina by thermal decomposition of AACH precursor using low temperature solid state reaction. Mater Res Bull. 2012;47:4271–7.
30. Peng LL, Xu XY, Lv Z, Song JQ. Thermal and morphological study of Al_2O_3 nanofibers derived from boehmite precursor. J Therm Anal Calorim. 2012;110:749–54.
31. Song JQ, Li ZH, Xu XY, He MY. Organic-free synthesis of boehmite nanofibers by $Al_2(SO_4)_3{\cdot}18H_2O$ with high pore volume. Ind Eng Chem Res. 2013;52:7752–7.
32. Xu XY, Liu YX, Lv Z, Song JQ, He MY. Thermal study of boehmite nanofibers with controlled particle size. J Therm Anal Calorim. 2014;115:1111–7.
33. Strek W, Deren P, Bednarkiewicz A. Cooperative processes in $KYb(WO_4)_2$ crystal doped with Eu^{3+} and Tb^{3+} ions. J Lumin. 2000;87:999–1001.
34. Zhang J, Shi FG, Lin J, Wei SY, Chen DF. Nanoparticles assembly of boehmite nanofibers without a surfactant. Mater Res Bull. 2008;43:1709–15.
35. Li GC, Guan LL, Liu YQ, Liu CG. Template-free solvothermal synthesis of 3D hierarchical nanostructured boehmite assembled by nanosheets. J Phys Chem Solids. 2012;73:1055–60.
36. Zhang LM, Lu WC, Cui RR, Shen SS. One-pot template-free synthesis of mesoporous boehmite core–shell and hollow spheres by a simple solvothermal route. Mater Res Bull. 2010;45:429–36.
37. Sarikaya Y, Onal M, Ada K. An indirect thermodynamic model developed for initial stage sintering of an alumina compacts by using porosity measurements. J Therm Anal Calorim. 2012;107:419–23.
38. Palmero P, Bonelli B, Lomello F, Garrone E, Montanaro L. Role of the dispersion route on the phase transformation of a nanocrystalline transition alumina. J Therm Anal Calorim. 2009;97:223–9.
39. Palmer SJ, Frost RL. Thermal decomposition of Bayer precipitates formed at varying temperatures. J Therm Anal Calorim. 2010;100:27–32.
40. Yoshida MI, Silva VR, Pinto PCC, Silva MC, Carvalho CF. Physico-chemical characterization and thermal analysis data of alumina waste from Bayer process. J Therm Anal Calorim. 2012;109:1429–33.
41. Hao LC, Yu WD. Evaluation of thermal protective performance of basalt fiber nonwoven fabrics. J Therm Anal Calorim. 2010;100:551–5.
42. Barbes B, Paramo R, Blanco E, Pineiro MM, Casanova C. Thermal conductivity and specific heat capacity measurements of Al_2O_3 nanofluids. J Therm Anal Calorim. 2013;111:1615–25.
43. Hirata G, Perea N, Tejeda M, McKittrick J. Luminescence study in Eu-doped aluminum oxide phosphors. Opt Mater. 2005;27:1311–5.